European Radiology (2020) 30:308–319
https://doi.org/10.1007/s00330-019-06319-0

MAGNETIC RESONANCE

Compressed sensing MRI of different organs: ready for clinical daily practice?

Bénédicte Marie Anne Delattre[1] · Sana Boudabbous[1] · Catrina Hansen[1] · Angeliki Neroladaki[1] · Anne-Lise Hachulla[1] · Maria Isabel Vargas[2]

Received: 11 April 2019 / Revised: 28 May 2019 / Accepted: 11 June 2019/ Published online: 1 July 2019

Abstract

Objectives The aim was to evaluate the image quality and sensitivity to artifacts of compressed sensing (CS) acceleration technique, applied to 3D or breath-hold sequences in different clinical applications from brain to knee.

Methods CS with an acceleration from 30 to 60% and conventional MRI sequences were performed in 10 different applications in 107 patients, leading to 120 comparisons. Readers were blinded to the technique for quantitative (contrast-to-noise ratio or functional measurements for cardiac cine) and qualitative (image quality, artifacts, diagnostic findings, and preference) image analyses.

Results No statistically significant difference in image quality or artifacts was found for each sequence except for the cardiac cine CS for one of both readers and for the wrist 3D proton density (PD)–weighted CS sequence which showed less motion artifacts due to the reduced acquisition time. The contrast-to-noise ratio was lower for the elbow CS sequence but not statistically different in all other applications. Diagnostic findings were similar between conventional and CS sequence for all the comparisons except for four cases where motion artifacts corrupted either the conventional or the CS sequence.

Conclusions The evaluated CS sequences are ready to be used in clinical daily practice except for the elbow application which requires a lower acceleration. The CS factor should be tuned for each organ and sequence to obtain good image quality. It leads to 30% to 60% acceleration in the applications evaluated in this study which has a significant impact on clinical workflow.

Key Points

- *Clinical implementation of compressed sensing (CS) reduced scan times of at least 30% with only minor penalty in image quality and no change in diagnostic findings.*
- *The CS acceleration factor has to be tuned separately for each organ and sequence to guarantee similar image quality than conventional acquisition.*
- *At least 30% and up to 60% acceleration is feasible in specific sequences in clinical routine.*

Keywords Magnetic resonance imaging · Acceleration · Image processing, computer-assisted · Data compression

Abbreviations

3D	Three-Dimensional
BTFE	Balanced turbo field echo
Cine	Cinematic sequence
CNR	Contrast-to-noise ratio
CS	Compressed sensing
FFE	Fast field echo
FLAIR	Fluid-attenuated inversion recovery
FOV	Field of view
mDixon	Multi-echo two-point Dixon
MRCP	Magnetic resonance cholangiopancreatography
MSK	Musculoskeletal
PD	Proton density
SENSE	Sensitivity encoding
SPAIR	Spectral attenuated inversion recovery

Electronic supplementary material The online version of this article (https://doi.org/10.1007/s00330-019-06319-0) contains supplementary material, which is available to authorized users.

✉ Bénédicte Marie Anne Delattre
benedicte.delattre@hcuge.ch

[1] Division of Radiology, Geneva University Hospitals, Rue Gabrielle-Perret-Gentil 4, 1211 Geneva 14, Switzerland

[2] Division of Neuroradiology, Geneva University Hospitals , Geneva, Switzerland

TSE Turbo spin echo
VISTA Volumetric isotropic T2w acquisition

Introduction

Acceleration methods are important for MRI, in the interest of examination time as well as image quality. They range from accelerated sequences (turbo spin echo (TSE), fast field echo (FFE)) to reconstruction methods such as parallel imaging. High-resolution and 3D imaging became feasible in a clinically reasonable time. In addition, imaging of moving organs clearly benefits from these techniques, as the challenge is to acquire images of reasonable quality during patient breath-hold. Nevertheless, acquisition time is still the main limiting factor in MRI.

Because MRI image is sparse when represented in an appropriate transform domain, data acquisition can be reduced, without nearly any penalty on the final reconstructed image. This promising technique is known as compressed sensing (CS) [1–3]. Nevertheless, it required some important technical efforts to bring it into clinics for several reasons [4]. One is the difficulty to predict which acceleration factor can be used since it depends on the original sequence and its signal-to-noise ratio. No rule can be surely derived to determine how far acquisition can be accelerated without image penalty. This point requires a clinical implementation with validated techniques, quantitative but most importantly qualitative in order to determine if a diagnostic feature would be different using CS and also if some new kind of artifacts were to be observed. This has already been performed by several groups in the previous years, for various separate applications [5] notably in the brain [6–9], vessels [10], body [11–15], heart including large vessels [16–19], breast [20], musculoskeletal (MSK) [21–23], and also pediatric [24] or even spectroscopic imaging [25, 26].

The aim of the present study was to evaluate the image quality and diagnostic findings of CS, applied to 3D or breath-hold sequences in different clinical applications from brain to knee.

Material and methods

A total of 107 patients between September 2017 and July 2018 were included in the study, leading to 120 comparisons between conventional and CS sequences. Patient inclusion was not consecutive but mainly based on patient compliance and time constraint in the clinical workflow and concerned patients referred for neurological, cardiac, abdominal, or MSK examination. No restriction about the exam indication was made. Details about patient population are given in Table 1.

MRI acquisition

Images were acquired on a 1.5-T Ingenia MRI (Philips) with release 5.4 including "compressed SENSE" option (using together CS and SENSE acceleration). In neuroradiologic imaging, 3D fluid-attenuated inversion recovery (FLAIR) and 3D FFE T1-weighted post contrast (gadoterate meglumine, Dotarem, Guerbet) injection were included in the study. Short-axis cardiac cinematic sequence (cine) centered in the middle of the cavity and acquired during breath-hold was investigated. In the abdomen, 3D magnetic resonance cholangiopancreatography (MRCP) with respiratory trigger for cholangiography as well as 3D FFE T1-weighted with a multi-echo two-point Dixon (mDixon) water-fat separation technique after contrast injection, acquired during breath-hold in transverse or coronal orientation, was evaluated. Also, 3D TSE T2-weighted (VISTA) sequence for the rectum was evaluated. Finally, in MSK, sequences investigated were 3D TSE proton density (PD)–weighted VISTA sequences with spectral attenuated inversion recovery (SPAIR) fat suppression for the wrist, the elbow, and the knee. Table 2 shows the sequence parameters. The time reduction for CS was chosen with the aim of nearly not degrading the image quality (based on preliminary testing of the sequences). The CS factor depends on the SENSE factor of the original sequence parameters; when CS is enabled in a conventional sequence, the SENSE parameter is not available anymore and the CS initial factor represents the SENSE acceleration (multiplication of both phase direction acceleration factors when in 3D), then increasing the CS factor further reduces the scan time. The % time reduction is indicated since it better represents the additional acceleration provided by CS. The regularization term used in the CS reconstruction is limited to three modes in the user interface: weak, medium, or strong. The "medium" mode was always used. CS sequence was always acquired after the conventional sequence, sometimes after the injection of contrast media, particularly for the cardiac MRI.

Qualitative image analysis

Images were anonymized in two sets (conventional and CS sequences) with random patient name. Images of each organ were first reviewed by one experienced radiologist in each field (22 years of experience for brain, 14 for heart, 9 for abdomen, 15 for MSK). The images were blinded from the acquisition technique and the patient identity and were presented to the radiologist, one set at a time, meaning that at the end of the session, all patients and both sequences (CS and conventional) were reviewed, but in a random order. The image quality was

Table 1 Details about patients included in the study separated for each different application and CS sequence evaluated. *BTFE* balanced turbo field echo, *SA* short axis

			No. of patients included	Age Mean [range] years
Neuro	Brain	3D FLAIR sagittal	19	60 [31–89]
		3D T1 TFE Gd sagittal	20	66 [31–85]
Cardiac	Heart	BTFE cine SA	14	38 [17–76]
Abdomen	Liver	3D T1 mDixon Gd transverse	14	59 [24–88]
		3D T1 mDixon Gd coronal	5	42 [18–69]
	Rectum	3D T2 VISTA coronal	9	58 [22–88]
	Bile duct	MRCP trig	7	64 [37–88]
MSK	Wrist	3D PD VISTA SPAIR coronal	12	38 [16–60]
	Elbow	3D PD VISTA SPAIR sagittal	6	34 [18–44]
	Knee	3D PD VISTA SPAIR sagittal	14	38 [17–76]

evaluated on a 5-point scale (1, excellent; 2, good; 3, sufficient for diagnostic; 4, bad but still diagnostic; 5, not interpretable). The radiologist was also asked to report any artifact in the image and its nature. After this first evaluation, the images were grouped by patient and presented together but still blinded to the acquisition technique. The radiologist was asked to compare the diagnostic findings on both images and to note if any difference was visible. Additionally, the preferred image was designated with a possibility to choose "no difference" if there was no clear preference.

A second blinded reader (with nine years of experience) evaluated independently the total number of patients included in the study using the same procedure (first reading one set at a time and second reading sequences grouped by patient) and evaluation criteria.

Quantitative image analysis

Contrast-to-noise ratio (CNR) was measured (by a physicist, 10 years of experience) on each sequence also in a blinded manner (for the acquisition technique), on the original images (no MIPs or reformatted images). The details about CNR measurement are given in supplementary material.

The CNR was measured for all sequences except for the cardiac cine because of the different timing after the contrast injection. For the cardiac sequences, quantitative measurements were performed in a blinded manner (by a radiologist with 14 years of experience) on the short-axis cine with cvi42 (Circle Cardiovascular Imaging Inc.). Volumes as well as ejection fraction for left and right ventricles and mass for left ventricle were computed following semi-automatic segmentation of the cavities and wall performed in the middle of the heart (the same position for the conventional and CS sequence).

Statistics

For image quality, the median was calculated and a paired Wilcoxon test was used to compare conventional and CS sequences, as well as for comparing the presence of artifact in the images. Cohen's kappa was calculated to estimate the agreement between both readers. For quantitative calculation (CNR and cardiac function parameters), a paired Wilcoxon test was used to compare sequences. All statistics were performed with R (RStudio, R version 3.3.2).

Results

The difference in image quality between conventional and CS sequences was very slight but statistically significant (Table 3, $p = 0.006$ for reader 1 and $p = 0.05$ for reader 2). When analyzed sequence by sequence, no significant difference of image quality for both readers was found between CS and conventional images except for heart cine for reader 1. Globally, the agreement between readers for the evaluation of the conventional or the CS sequences was fair ($\kappa = 0.30$ and $\kappa = 0.25$ respectively). The presence of artifacts, and in particular motion artifact, is listed in Table 3. The latter was analyzed separately since one can hypothesize that CS sequences would be less prone to motion artifacts. Overall, the artifacts found by both readers can be classified as artifacts due to the presence of metal, suboptimal fat suppression, motion artifact (including respiratory artifacts), and noise and folding artifact. There was no difference in the occurrence of artifacts between conventional versus CS when all organs were pooled together but also when analyzed separately (except for 3D PD SPAIR for reader 2). The agreement between readers for the detection of artifacts was globally moderate ($\kappa = 0.39$ for conventional and $\kappa = 0.47$ for CS). When

Table 2 MRI parameters of the conventional and CS-accelerated sequences evaluated in this study. Note that the CS factor itself does not indicate the acceleration in a straightforward manner, since it depends on the original sequence, this is the reason why the % time reduction is indicated. *FOV* field of view

	Common sequence parameters			
	Conventional sequence		CS sequence	
	SENSE factor	Acquisition time	CS factor	Acquisition time % time reduction
Brain 3D T1 TFE Gd	Sagittal orientation, FOV 256 × 238 mm^2, acq voxel size 1.05 × 1.10 × 1.10 mm^3, rec voxel size 0.64 × 0.64 × 0.55 mm^3, slices 290, flip angle 8°, TE/TR 3.5/7.5 ms, TI 842 ms.			
	Phase (AP) 1, Slice (RL) 2	5 min 8 s	2.8	3 min 5 s 40%
Brain 3D FLAIR	Sagittal orientation, FOV 250 × 241 mm^2, acq voxel size 1.30 × 1.29 × 1.2 mm^3, rec voxel size 0.78 × 0.78 × 0.60 mm^3, slices 291, fat suppression SPIR, 3D view "Brain FLAIR", TE/TR 297/4800 ms (TE equ. 133 ms), TI 1660 ms.			
	Phase (AP) 2, Slice (RL) 1.8	5 min 31 s	5.3	4 min 27%
Heart sBTFE cine	Short-axis orientation, FOV 350 × 302 mm^2, acq voxel size 1.68 × 2.04 × 8.00 mm^3, rec voxel size 0.99 × 0.99 × 8.00 mm^3, slices 2, fa 60°, TE/TR 1.46/2.9 ms.			
	Phase (AP) 2.5	11.4 s (for heart rate 95 bpm)	5	6.3 s (for heart rate 95 bpm) 45%
Bile duct MRCP trig	Transverse orientation, FOV 260 × 260 mm^2, acq voxel size 1.10 × 1.20 × 1.50 mm^3, rec voxel size 0.65 × 0.65 × 0.75 mm^3, slices 120, fat suppression SPIR, 3D view "no", TE/TR 500/687 ms (TE equ. 435 ms).			
	Phase (RL) 1.7, Slice (AP) 1.4	4 min 33 s (respiratory trigger)	9	1 min 48 s (respiratory trigger) 60%
Liver 3D T1 mDixon Gd	Transverse orientation, FOV 420 × 357 mm^2, acq voxel size 1.50 × 1.87 × 4.00 mm^3, rec voxel size 0.88 × 0.88 × 2.00 mm^3, slices 110, fa 15°, TE1/TE2/TR 1.8/4.0/5.8 ms.			
	Phase (AP) 2, Slice (FH) 1.8	13.5 s	6	8.9 s 36%
Liver 3D T1 mDixon Gd	Coronal orientation, FOV 450 × 418 mm^2, acq voxel size 2.01 × 1.99 × 4.00 mm^3, rec voxel size 1.00 × 1.00 × 2.00 mm^3, slices 100, fa 15°, TE1/TE2/TR 1.8/4.0/5.7 ms.			
	Phase (RL) 2, Slice (AP) 2	12.6 s	6	9.4 s 31%
Rectum 3D T2 VISTA	Coronal orientation, FOV 300 × 300 mm^2, acq voxel size 0.90 × 0.93 × 0.90 mm^3, rec voxel size 0.78 × 0.78 × 0.90 mm^3, slices 222, 3D view "no", TE/TR 120/2000 ms.			
	Phase (RL) 2, Slice (AP) 1.5	7 min 56 s	4.2	5 min 8 s 35%
Elbow 3D PD VISTA SPAIR	Sagittal orientation, FOV 122 × 122 mm^2, acq voxel size 0.50 × 0.56 × 0.60 mm^3, rec voxel size 0.28 × 0.28 × 0.30 m^3, slices 300, fat suppression SPAIR, 3D view "MSK PD FS", TE/TR 27/1300 ms			
	Phase (AP) 1.5, Slice (RL) 1.5	6 min 11 s	3.5	4 min 8 s 33%
Wrist 3D PD VISTA SPAIR	Coronal orientation, FOV 100 × 100 mm^2, acq voxel size 0.40 × 0.45 × 0.50 mm^3, rec voxel size 0.30 × 0.30 × 0.25 m^3, slices 282, fat suppression SPAIR, 3D view "MSK PD FS", TE/TR 29/1300 ms			
	Phase (AP) 1.5, Slice (RL) 1.5	6 min 50 s	3.5	4 min 37 s 32%
Knee 3D PD VISTA SPAIR	Sagittal orientation, FOV 140 × 159 mm^2, acq voxel size 0.55 × 0.66 × 0.70 mm^3, rec voxel size 0.40 × 0.40 × 0.35 m^3, slices 500, fat suppression SPAIR, 3D view "no", TE/TR 28/1250 ms			
	Phase (AP) 1.5, Slice (RL) 1.5	6 min 11 s	3.5	4 min 8 s 33%

evaluated next to each other, the preferred sequence for each reader is reported in Table 4. Quantitative results such as CNR measured in conventional and CS sequences are shown in Fig. 1. Cardiac quantitative measurements performed on cine are shown in Table 5. The following results are described separately according to each organ. Figure 2 shows examples of images obtained for all evaluated applications.

Brain MRI

No statistical difference was found between conventional and CS in image quality or occurrence of artifacts. Reader 1 found significantly more motion artifacts than reader 2 for contrast-enhanced 3D T1. This was due to a difference of appreciation of the motion artifact; indeed, reader 1 mentioned even very slight motion observed at the top of the brain whereas reader 2 mentioned only large bulk motion artifacts. There was a marked preference for the conventional sequence for reader 1 whereas reader 2 did not mention such a preference. Indeed, for contrast-enhanced 3D T1, CS exhibited globally less noise in the white matter area and a blurrier transition between the white and gray matter, which is illustrated in Fig. 3. For 3D FLAIR sequence, Fig. 4 illustrates the different features of CS with globally less noise but also less visibility of very small structures. This was however not impairing the ability to detect lesions in the sequence since both readers did not find diagnostic difference in any patient. This was also not confirmed by CNR measurements which were very similar between conventional and CS.

Heart cine MRI

Reader 1 found a significantly lower image quality of the CS cine sequence ($p = 0.020$), which was rated more often as "2, good" instead of "1, excellent." Reader 2 found both sequences as "1, excellent." The presence of artifacts was not different between sequences with a moderate agreement between readers ($\kappa = 0.44$). When analyzed together, there was no marked preference for any of both sequences, and this for both readers. Diagnostic findings were the same, except for one case for reader 1 due to motion artifact on CS. Quantitative measurements were very similar as shown in Table 5.

Abdominal MRI

For the four evaluated sequences, no significant difference in image quality or presence of artifact was found. Both readers showed a moderate to substantial agreement concerning the presence of motion artifacts for the MRCP sequence ($\kappa = 1$ for conventional and $\kappa = 0.7$ for CS) as well as for the 3D T1 in transverse orientation ($\kappa = 0.53$ for CS and $\kappa = 0.59$ for conventional), meaning that they were easily recognized. The CNR was not different across sequences despite a tendency to be higher for CS than conventional, especially for MRCP.

MRCP

The preferred sequence was more often the conventional for both readers even though the diagnostic findings were similar. Indeed, there is a slightly less good visibility of fine structures in the CS sequence. MRCP was the most accelerated in our study with a time reduction of 60%. The detection of abnormal small structures could therefore be impaired with such a high acceleration factor.

Liver contrast–enhanced 3D T1 transverse and coronal sequences

Reader 1 preferred the conventional sequence while reader 2 had most often no preference. Finally, diagnostic findings were identical except for one case for both readers and an additional case for reader 1 (in transverse orientation). Indeed, for one of the two patients, CS was acquired at a late phase after contrast medium injection which makes a comparison difficult for both readers. Reader 1 mentioned also too much respiration artifacts for interpretation of the CS sequence. Concerning the other patient, only reader 1 found a possible mild dilatation of intrahepatic bile ducts on conventional sequence that was not visible on CS, and mentioned that conventional sequence was prone to motion artifacts. Considering the other sequences of the exam, the ectasia was due to the artifacts and not real.

Rectum 3D T2 VISTA sequence

Nearly no artifacts were observed for this sequence. There was mainly no preference between conventional and CS when looked one next to each other even though reader 1 described a slight blurriness on small structures of CS in nearly 30% of cases. Figure 5 illustrates this for one patient.

MSK MRI

The image quality was not significantly different between conventional and CS for the three sequences evaluated, with a moderate to nearly perfect agreement between readers for wrist and knee.

Elbow 3D PD SPAIR sequence

The presence of artifacts was similar; however, both readers preferred more often conventional sequence than CS. Despite this difference, the diagnostic was identical between both sequences. CNR was significantly lower for CS ($p = 0.031$).

Wrist 3D PD SPAIR sequence

The artifacts were (significantly for reader 2, $p = 0.037$) more present in conventional sequence (mainly motion) with a perfect agreement between readers ($\kappa = 0.82$ for conventional and $\kappa = 1$ for CS). Both readers often found no preference between sequences or a preference

Table 3 Median with range in brackets as well as mean ± SD image quality (A) and occurrence of artifacts (B) and, in particular, motion artifacts in brackets. Result of the Wilcoxon paired test is given for the comparison between methods, and kappa is given for the agreement between readers (global agreement with all the applications together is mentioned at the bottom of the table for each sequence). Significant differences ($p < 0.05$) are indicated in italic.

		Reader 1			Reader 2			Agreement between readers (κ)	
	n	Conventional	CS	*p* value	Conventional	CS	*p* value	Conventional	CS
A. Median image quality									
Brain 3D T1 Gd	20	2 [1–5], 2.2 ± 0.8	2 [2–5], 2.4 ± 0.8	0.299	1.5 [1–5], 1.8 ± 1.1	2 [1–4], 2.0 ± 0.9	0.267	0.16	0.32
Brain 3D FLAIR	19	2 [1–3], 2.0 ± 0.3	2 [1–5], 2.1 ± 0.9	0.824	2 [1–3], 1.6 ± 0.7	2 [1–4], 1.7 ± 0.8	0.777	0.20	0.32
Heart cine	14	1 [1–4], 1.2 ± 0.8	1.5 [1–4], 1.6 ± 0.8	*0.020*	1 [1–3], 1.3 ± 0.6	1 [1–3], 1.4 ± 0.6	0.766	0.21	0.48
Bile duct MRCP trig	7	3 [1–4], 2.9 ± 1.1	3 [3–4], 3.4 ± 0.5	0.346	2 [1–2], 1.7 ± 0.5	2 [1–3], 2.0 ± 0.6	0.346	0.17	− 0.09
Liver 3D T1 Gd tra	14	2 [1–4], 2.0 ± 1.0	2.5 [1–5], 2.7 ± 1.6	0.163	2 [1–4], 1.9 ± 1.0	2 [1–4], 2.1 ± 1.2	0.440	0.59	0.16
Liver 3D T1 Gd cor	5	3 [1–5], 3.0 ± 1.6	3 [1–5], 3.2 ± 1.5	1.000	2 [1–3], 1.8 ± 0.8	2 [1–3], 2.0 ± 0.7	1.000	− 0.25	0.09
Rectum 3D T2 VISTA	9	3 [1–4], 2.7 ± 1.0	3 [1–4], 2.8 ± 1.0	1.000	1 [1–2], 1.4 ± 0.5	2 [1–2], 1.6 ± 0.5	0.773	− 0.12	− 0.08
Elbow 3D PD SPAIR	6	1 [1–4], 1.8 ± 1.3	2.5 [1–4], 2.3 ± 1.2	0.371	2 [1–3], 1.8 ± 0.8	2 [1–3], 1.8 ± 0.8	1.000	0.11	0.11
Wrist 3D PD SPAIR	12	1 [1–3], 1.6 ± 0.8	1 [1–2], 1.4 ± 0.5	0.530	2 [1–3], 1.8 ± 0.8	2 [1–2], 1.8 ± 0.5	1.000	0.47	0.77
Knee 3D PD SPAIR	14	1 [1–2], 1.2 ± 0.4	1 [1–3], 1.4 ± 0.6	0.424	1 [1–2], 1.3 ± 0.5	1 [1–2], 1.3 ± 0.5	1.000	0.81	0.50
All sequences	120	2 [1–5], 1.9 ± 1.0	2 [1–5], 2.2 ± 1.2	*0.006*	1 [1–5], 1.6 ± 0.8	2 [1–4], 1.7 ± 0.8	*0.05*	0.30	0.25
B. Artifact all types (in brackets motion artifact)									
Brain 3D T1 Gd	20	16 (14)	18 (14)	0.42 (1)	5 (5)	9 (9)	0.129 (0.129)	0.15 (0.25)	0.17 (0.33)
Brain 3D FLAIR	19	9 (5)	6 (2)	0.351 (1)	2 (1)	1 (1)	1 (1)	0.012 (0.27)	0.21 (0.64)
Heart cine	14	1 (0)	3 (2)	0.35 (0.35)	3 (0)	1 (0)	0.346 (1)	0.44 (1)	0.44 (0)
Bile duct MRCP trig	7	3 (2)	3 (2)	1 (1)	2 (2)	3 (3)	1 (1)	0.7 (1)	0.42 (0.7)
Liver 3D T1 Gd tra	14	7 (6)	10 (9)	0.23 (0.23)	7 (3)	9 (6)	0.424 (0.233)	0.71 (0.53)	0.19 (0.59)
Liver 3D T1 Gd cor	5	2 (0)	2 (1)	1 (1)	2 (2)	2 (2)	1 (1)	0.17 (0)	0.17 (0.55)
Rectum 3D T2 VISTA	9	1 (0)	0 (0)	1 (1)	0 (0)	0 (0)	1 (1)	0 (1)	1 (1)
Elbow 3D PD SPAIR	6	2 (0)	3 (1)	1 (1)	4 (0)	4 (1)	1 (1)	0.4 (1)	0 (− 0.2)
Wrist 3D PD SPAIR	12	4 (4)	0 (0)	0.072 (0.072)	5 (4)	0 (0)	*0.037* (0.072)	0.82 (0.63)	1 (1)
Knee 3D PD SPAIR	14	2 (1)	1 (1)	1 (1)	4 (0)	1 (0)	0.149 (1)	0.59 (0)	1 (0)
All sequences	120	47 (32)	46 (32)	0.87 (1)	34 (17)	30 (22)	0.44 (0.26)	0.39 (0.47)	0.47 (0.57)

for CS. Diagnostic findings were similar, except in one case for reader 1, for which the conventional sequence had important motion artifacts. The CNR was slightly higher for CS compared with that of the conventional (not significant, $p = 0.064$).

Knee 3D PD SPAIR sequence

The presence of artifacts was also similar between sequences, with a moderate to perfect agreement between readers ($k = 0.59$ for conventional and $k = 1$ for CS). In most cases, both readers did not find a preference for the CS or for the conventional sequence. No difference in diagnostic findings was noted and the CNR was identical.

Discussion

CS acceleration is not a new technique; however, its practical use in clinical routine is quite recent even though an already large number of published studies demonstrated the advantages of the CS technique [4, 5]. In this study, we have shown

Table 4 Occurrence of the preferred sequence for both readers, either conventional, CS, or no preference between both

		Reader 1			Reader 2		
Preferred sequence	*n*	Conventional	CS	No difference	Conventional	CS	No difference
Brain 3D T1 Gd	20	16	1	3	5	4	11
Brain 3D FLAIR	19	10	5	4	4	2	13
Heart cine	14	3	0	11	4	1	9
Bile duct MRCP trig	7	5	0	2	4	1	2
Liver 3D T1 Gd tra	14	8	4	2	4	3	7
Liver 3D T1 Gd cor	5	2	1	2	0	2	3
Rectum 3D T2 VISTA	9	3	1	5	0	1	8
Elbow 3D PD SPAIR	6	4	0	2	5	0	1
Wrist 3D PD SPAIR	12	0	4	8	1	2	9
Knee 3D PD SPAIR	14	2	3	9	1	1	12
All sequences	120	53	19	48	28	17	76

that with CS, image quality and artifacts were similar. Diagnosis was identical except in four patients where conventional and/or CS sequences was corrupted by motion artifacts. Concerning artifacts, CS did not exhibit different or new artifacts compared with conventional sequences, which is an important information. A recent study described in details some particular artifacts with CS sequences encountered especially on low signal-to-noise ratio sequences [27] which were not observed in our study.

One difference that was noted was either a slightly noisier aspect of CS (for bile duct, or for cardiac cine for example), or on the contrary a smoother aspect of the image (for brain 3D FLAIR for example). This is probably due to the fine tuning of the regularization term used in the CS reconstruction which is limited to three modes in the user interface: weak, medium, or strong. Some previous empirical experiences in our center showed that the "medium" mode was always preferred (either too noisy for the "weak" or too flat with a synthetic aspect for the "strong" modes). Moreover, the presence of noise also directly depends on the acceleration factor which has to be evaluated sequence by sequence. Clearly, for 3D PD VISTA SPAIR in elbow, our results showed that CS was of lower quality. Conversely, for wrist 3D PD VISTA SPAIR sequence, CS was better rated than conventional; however, in both cases, a ~30% time reduction was applied. This confirms that CS acceleration level should be evaluated separately for each specific sequence and each organ.

Some previously published studies showed equivalent results. For the brain, a study demonstrated that in 2D T2 FSE and FLAIR, CS introduces a slight blurring for acceleration factor higher than two which prevented a good delineation of fine structures such as the hippocampus [28]. Another study showed very similar performances of CS for 3D T1 and 3D FLAIR sequences with acceleration factors of 35% and 25% respectively [6]. For cardiac imaging, a study showed a nice correlation of results for left ventricle functional parameters between CS and conventional sequences. Here the acceleration was higher than that in our study (80% reduction factor), but with slightly different acquisition parameters between both sequences [18]. For MSK, a study showed that for 3D TSE imaging of the knee, CS provided an adequate image quality with a significant time reduction (37%); however, authors also mentioned blurrier images, notably in the delineation of cartilage and subchondral bone [29]. Another study compared the performance of 3D T2 FSE with CS and found also a very good performance with 30% acceleration [30]. Concerning abdominal imaging, a study compared the performance of respiratory-triggered MRCP with and without CS acceleration. This study was performed with approximately 50% reduction in the acquisition time. The authors did not find significant differences in image quality between both sequences [14]. The common factor to a large number of these previously published studies is that CS was evaluated (and more often developed) for one particular application. Here, we have used the vendor implementation of CS acceleration which is available for (nearly) all sequences and clinical applications. The reconstruction framework is therefore similar and not specifically tailored sequence by sequence. This renders the CS method very easy to use in the clinical workflow.

A limitation of our study was that the sequence with CS acceleration was always acquired at the end of the examination, sometimes a long time after the contrast injection. For this particular reason, the contrast of both series was often different for cardiac cine and for liver. However, this bias has not impaired the conclusions drawn concerning image quality and presence of artifacts. The blurring, which is a known drawback of CS, was not assessed quantitatively. The kappa calculation was also not always very appropriate

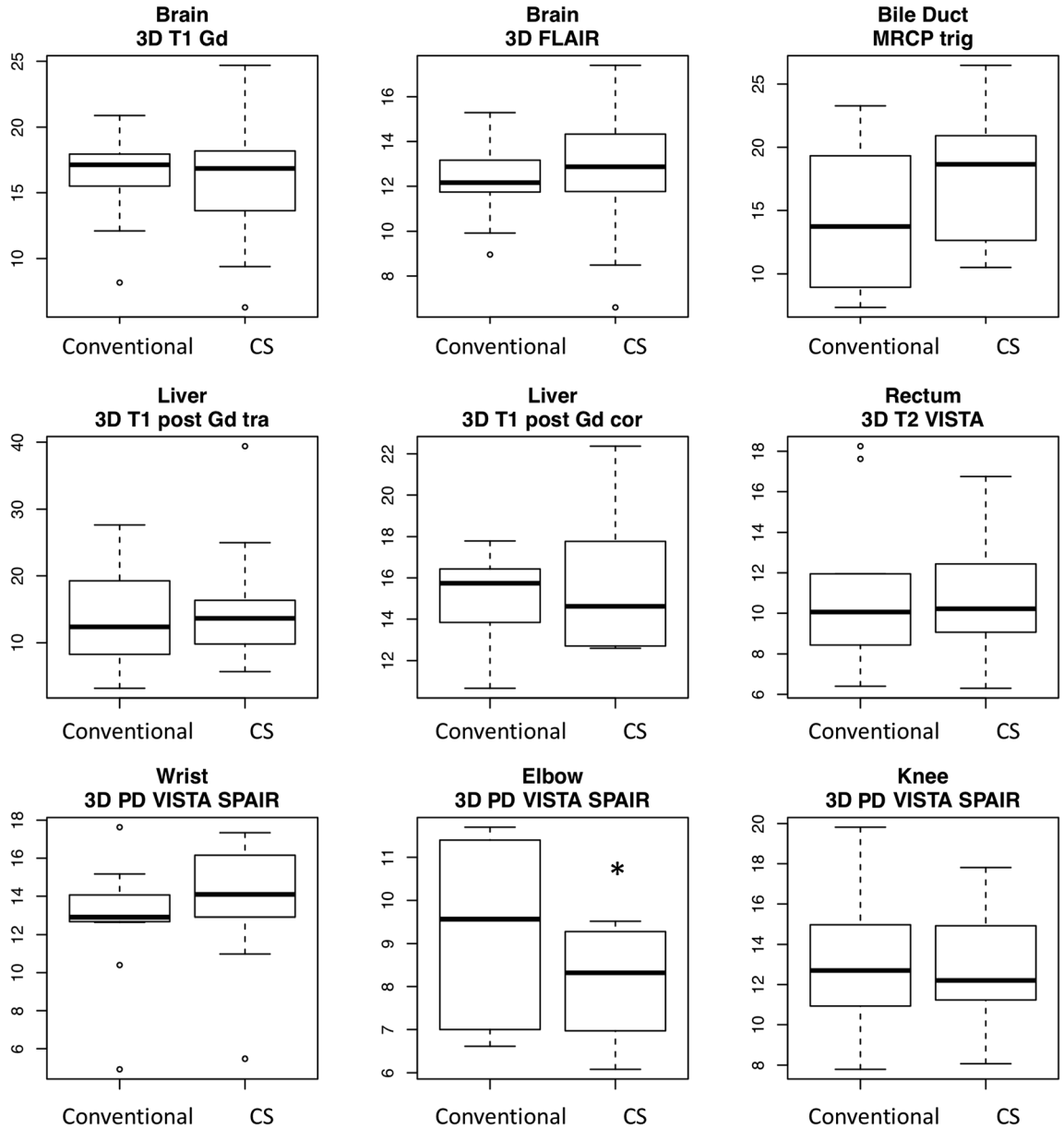

Fig. 1 CNR results for conventional or CS for each sequence evaluated; asterisk symbol indicates statistical difference ($p < 0.05$). Boxplot represents the median as bold line and 1st and 3rd quartiles are the limit of the box. Notches extend to ± 1.58 *interquartile range/$\sqrt{n}$ which corresponds to the 95% confidence interval; outliers are represented with circles; these are the default setting in R

due to the low number of observations in some applications (i.e., liver 3D T1 Gd coronal $n = 5$ or elbow $n = 6$). Finally, one must consider that differences found on this small number of patients may not reflect the whole general situation. Indeed,

Table 5 Results (mean ± SD) of quantitative measurements on middle slice of the cardiac cine for CS and conventional sequences

		p	Mean (CS-Conv.)	SD (CS-Conv.)	Mean ((CS-Conv.)/Conv.)
Left ventricle	End diastolic volume (ml)	0.542	0.11	0.69	0.70%
	End systolic volume (ml)	0.196	0.19	0.62	− 3.20%
	Ejection fraction %	0.093	− 1.31	2.45	2.40%
	Mass (g)	0.727	− 0.11	1.10	0.90%
Right ventricle	End diastolic volume (ml)	0.753	0.22	1.17	− 0.60%
	End systolic volume (ml)	0.638	0.15	0.97	− 0.30%
	Ejection fraction %	0.463	0.10	2.93	− 0.10%

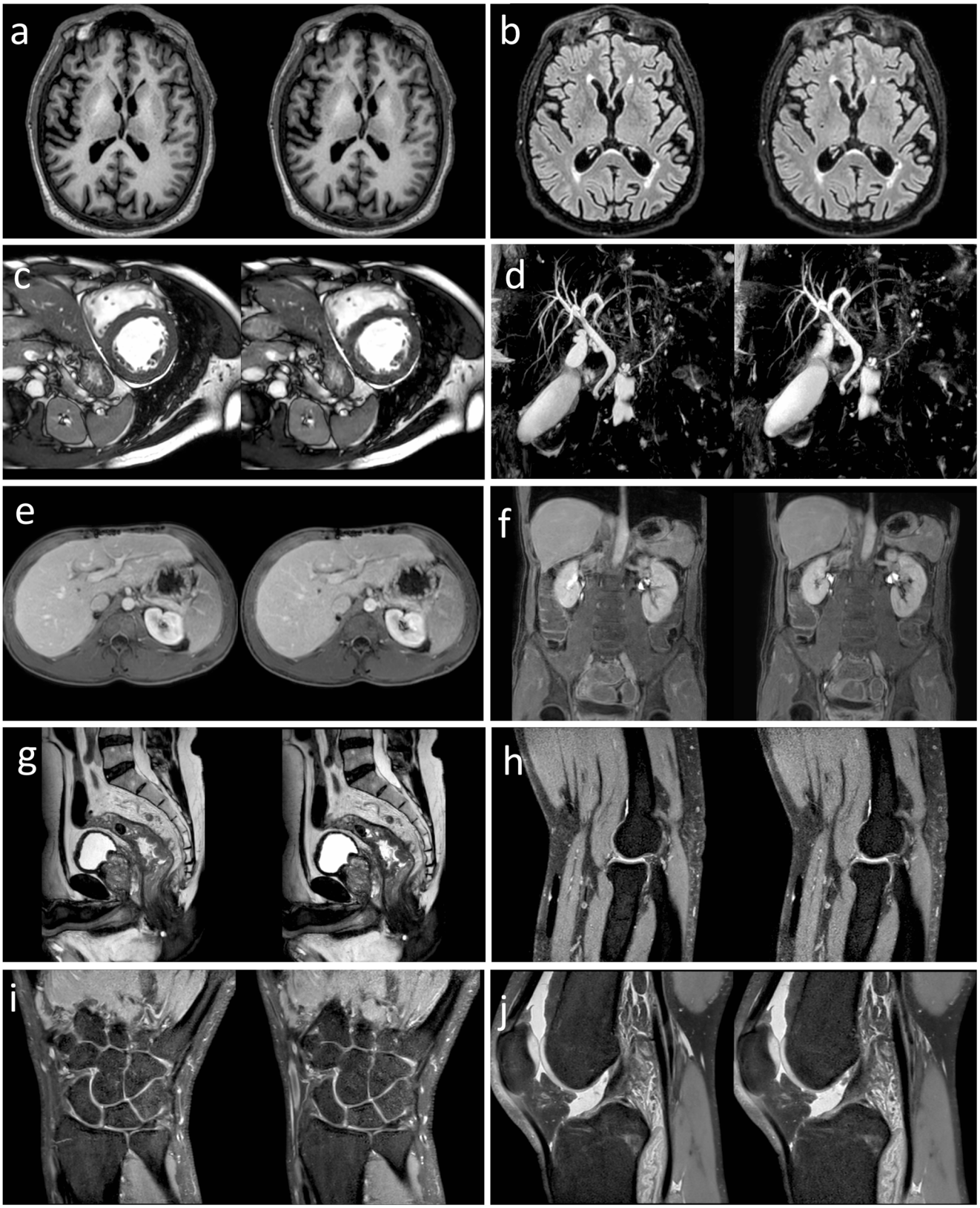

Fig. 2 Examples of images obtained with conventional (left) vs CS sequences (right) for all the applications tested, i.e. **a** Brain 3D T1 Gd (transverse reformat). **b** Brain 3D FLAIR (transverse reformat). **c** Heart cine. **d** Bile duct MRCP trig (maximum intensity projection). **e** Liver 3D T1 post Gd tra. **f** Liver 3D T1 post Gd cor. **g** Rectum 3D T2 VISTA (sagittal reformat). **h** Elbow 3D PD SPAIR. **i** Wrist 3D PD SPAIR. **j** Knee 3D PD SPAIR. The reformat orientation is shown for brain and rectum since it was the preferred orientation for interpretation

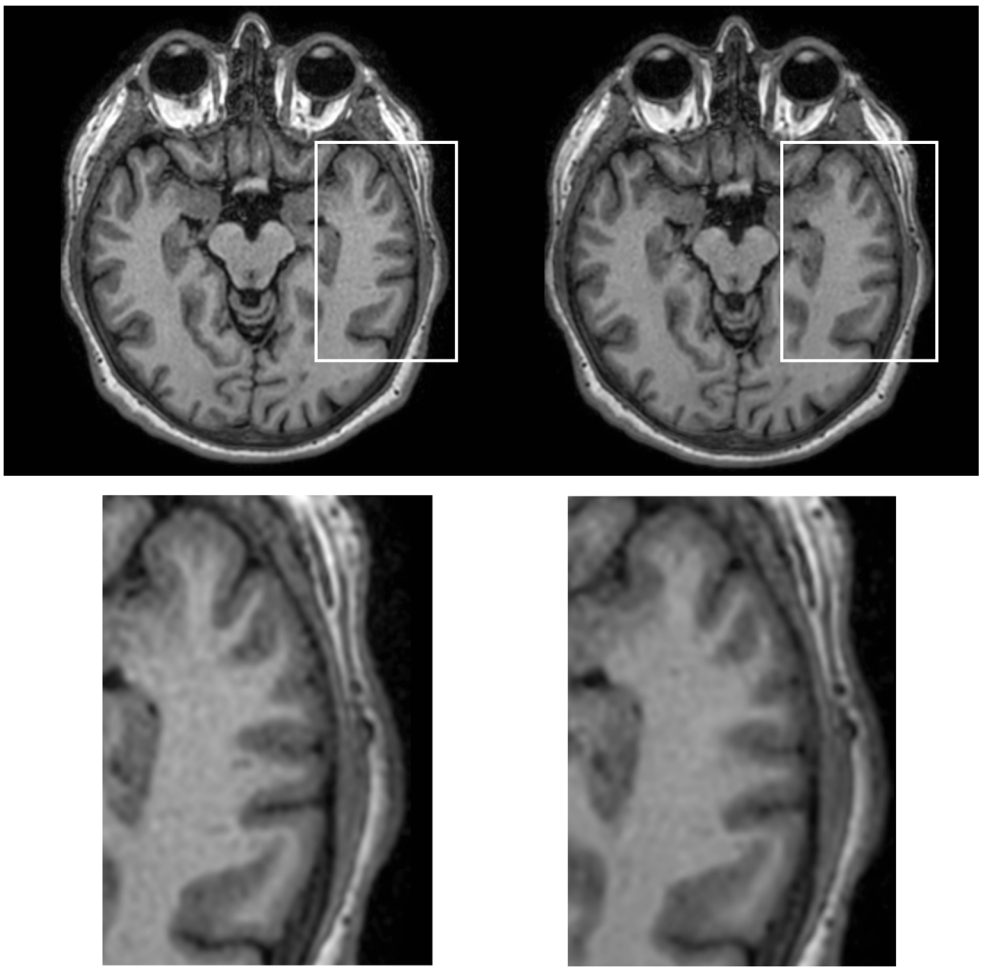

Fig. 3 Brain 3D T1 Gd sequence reformatted in transverse orientation. Conventional (left) versus CS (right). The global aspect of the CS sequence is less noisy than the conventional; however, the transition between white matter and gray matter is slightly blurrier on CS sequence (see zoom at bottom)

some small features were analyzed in our population but we cannot exclude that the blurring introduced by CS method may, in some cases, prevent some image findings to be clearly seen. Moreover, other methods can help reducing the image acquisition time such as reducing spatial resolution and increasing parallel imaging factors. In this study, we did not attempt to compare all the possible way of accelerating image acquisition but only to evaluate the result of CS acceleration on sequences that were already optimized for clinical routine, with the aim of not degrading substantially the image quality.

Finally, the choice of the acceleration factor was based on some previous pilot experience but the image quality is difficult to predict with a higher acceleration factor. Another study design could have been to separate the patients into two

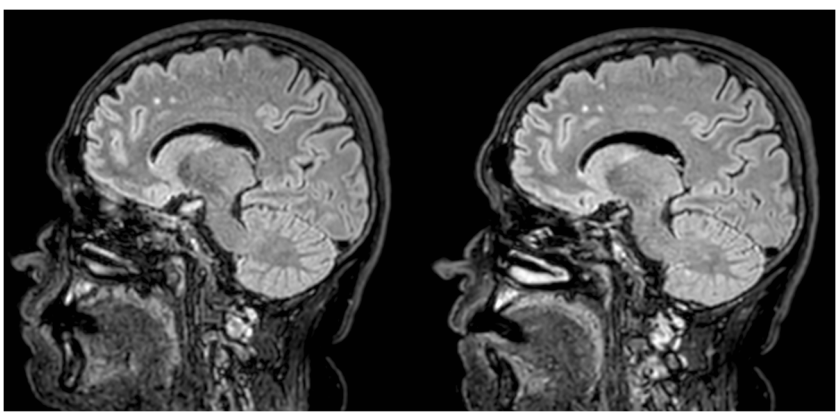

Fig. 4 Brain 3D FLAIR sequence, conventional (left) versus CS (right). This example illustrates the different aspects of CS sequence with globally less noise but also less visibility of very small structures (see the cerebellum for example). Note that the white matter lesions in the frontal lobe are well visible on both sequences

Fig. 5 Rectum 3D T2 VISTA conventional (left) versus CS (right) sequences. This example illustrates the situation of 30% of cases where small structures (white arrows) were less well depicted on the CS sequence

groups, one having a high acceleration factor (between 40 and 60%) and the other one having a lower acceleration factor such as what was done in this study.

Clinical implementation of the CS sequences evaluated

According to our results, all CS sequences can directly be used in clinical routine, except the elbow 3D PD SPAIR sequence which has to be less accelerated. Brain contrast–enhanced 3D T1 sequence was described as very good for a wide range of applications; however, due to the image blurriness observed at the white matter-gray matter border, clinical indications aiming at detecting very subtle changes in cortico-subcortical areas as epilepsy should be performed with conventional sequence. For the cardiac cine sequence, the 45% reduction in acquisition time saves numerous breath-holds to the patient. For abdominal sequences, the reduction in breath-hold time could clearly improve patient compliance without any penalty in image quality. The 60% accelerated bile duct MRCP sequence allowed a similar image quality with a limitation only when the indication of the exam concerns very distal biliary tracts. Finally, the wrist 3D PD SPAIR sequence clearly benefited from CS with less motion artifact in the sequence.

In conclusion, CS with an adequate acceleration factor is ready for clinical daily practice, providing similar image quality and occurrence of artifacts as compared with conventional sequences. A fine tuning of the acceleration factor is an important and necessary step before confident use of CS; however, this effort is rewarding since at least a 30% time reduction of sequences for routine examinations can be anticipated, with an obvious direct impact on clinical workflow.

Acknowledgments The authors want to thank Philips for having provided the compressed SENSE option, the whole technician team for their implication in the sequence tuning and acquisition, in particular Ms. Mahjabeen Bontean and M. Cédric Garcia, as well as Prof. Rares Salomir for his help with acquisition and data management for the abdominal images. We also gratefully thank the editor-in-chief Prof. Yves Menu and anonymous reviewers for their helpful comments.

Funding The authors state that this work has not received any funding.

Compliance with ethical standards

Guarantor The scientific guarantor of this publication is Prof. Maria Isabel Vargas.

Conflict of interest The authors of this manuscript declare no relationships with any companies, whose products or services may be related to the subject matter of the article.

Statistics and biometry No complex statistical methods were necessary for this paper.

Informed consent Written informed consent was waived by the Institutional Review Board.

Ethical approval Institutional Review Board approval was obtained (CCER 2016-01821).

Methodology
- retrospective
- cross-sectional study
- performed at one institution

References

1. Lustig M, Donoho DL, Santos JM, Pauly JM (2008) Compressed sensing MRI: a look at how CS can improve on current imaging techniques. IEEE Signal Process Mag 25:72–82
2. Lustig M, Donoho D, Pauly JM (2007) Sparse MRI: the application of compressed sensing for rapid MR imaging. Magn Reson Med 58:1182–1195
3. Liang D, Liu B, Wang J, Ying L (2009) Accelerating SENSE using compressed sensing. Magn Reson Med 62:1574–1584
4. Hollingsworth KG (2015) Reducing acquisition time in clinical MRI by data undersampling and compressed sensing reconstruction. Phys Med Biol 60:R297–R322
5. Jaspan ON, Fleysher R, Lipton ML (2015) Compressed sensing MRI: a review of the clinical literature. Br J Radiol 88:1–12

6. Vranic JE, Cross NM, Wang Y, Hippe DS, de Weerdt E, Mossa-Basha M (2019) Compressed sensing – sensitivity encoding (CS-SENSE) accelerated brain imaging : reduced scan time without reduced image quality. AJNR Am J Neuroradiol 40(1):92–98
7. Suh CH, Jung SC, Lee HB, Cho SJ (2019) High-resolution magnetic resonance imaging using compressed sensing for intracranial and extracranial arteries: comparison with conventional parallel imaging. Korean J Radiol 20:487–497
8. Eichinger P, Hock A, Schön S et al (2019) Acceleration of double inversion recovery sequences in multiple sclerosis with compressed sensing. Invest Radiol 54:319–324
9. Kayvanrad M, Lin A, Joshi R, Chiu J, Peters T (2016) Diagnostic quality assessment of compressed sensing accelerated magnetic resonance neuroimaging. J Magn Reson Imaging 44:433–444
10. Okuchi S, Fushimi Y, Okada T et al (2018) Visualization of carotid vessel wall and atherosclerotic plaque: T1-SPACE vs. compressed sensing T1-SPACE. Eur Radiol. https://doi.org/10.1007/s00330-018-5862-8
11. Feng L, Benkert T, Block KT, Sodickson DK, Otazo R, Chandarana H (2017) Compressed sensing for body MRI. J Magn Reson Imaging 45:966–987
12. Kwon H, Reid S, Kim D, Lee S, Cho J, Oh J (2017) Diagnosing common bile duct obstruction : comparison of image quality and diagnostic performance of three-dimensional magnetic resonance cholangiopancreatography with and without compressed sensing. Abdom Radiol (NY) 43:2255–2261
13. Nam JG, Lee JM, Lee SM et al (2019) High acceleration three-dimensional T1-weighted dual echo Dixon hepatobiliary phase imaging using compressed sensing-sensitivity encoding : comparison of image quality and solid lesion detectability with the standard T1-weighted sequence. Korean J Radiol 20:438–448
14. Yoon JH, Lee SM, Kang H-J et al (2017) Clinical feasibility of 3-dimensional magnetic resonance cholangiopancreatography using compressed sensing: comparison of image quality and diagnostic performance. Invest Radiol 52:612–619
15. Kawai N, Goshima S, Noda Y et al (2019) Gadoxetic acid-enhanced dynamic magnetic resonance imaging using optimized integrated combination of compressed sensing and parallel imaging technique. Magn Reson Imaging 57:111–117
16. Kamesh Iyer S, Tasdizen T, Burgon N et al (2016) Compressed sensing for rapid late gadolinium enhanced imaging of the left atrium : a preliminary study. Magn Reson Imaging 34:846–854
17. Basha TA, Akçakaya M, Liew C et al (2017) Clinical performance of high-resolution late gadolinium enhancement imaging with compressed sensing. J Magn Reson Imaging 46:1829–1838
18. Lin ACW, Strugnell W, Riley R et al (2017) Higher resolution cine imaging with compressed sensing for accelerated clinical left ventricular evaluation. J Magn Reson Imaging 45:1693–1699
19. Ma LE, Markl M, Chow K et al (2019) Aortic 4D flow MRI in 2 minutes using compressed sensing, respiratory controlled adaptive k-space reordering, and inline reconstruction. Magn Reson Med 81:3675–3690
20. Vreemann S, Rodriguez-Ruiz A, Nickel D et al (2017) Compressed sensing for breast MRI. Invest Radiol 52:574–582
21. Kijowski R, Rosas H, Samsonov A, King K, Peters R, Liu F (2017) Knee imaging: rapid three-dimensional fast spin-echo using compressed sensing. J Magn Reson Imaging 45:1712–1722
22. Wang N, Badar F, Xia Y (2017) Compressed sensing in quantitative determination of GAG concentration in cartilage by microscopic MRI. Magn Reson Med 79:3163–3171
23. Yi J, Lee YH, Hahn S, Albakheet SS, Song HT, Suh JS (2019) Fast isotropic volumetric magnetic resonance imaging of the ankle: acceleration of the three-dimensional fast spin echo sequence using compressed sensing combined with parallel imaging. Eur J Radiol 112:52–58
24. Vasanawala SS, Alley MT, Hargreaves BA, Barth RA, Pauly JM, Lustig M (2010) Improved pediatric MR imaging with compressed sensing. Radiology 256:607–616
25. Santos-Díaz A, Noseworthy MD (2019) Comparison of compressed sensing reconstruction algorithms for 31P magnetic resonance spectroscopic imaging. Magn Reson Imaging 59:88–96
26. Klauser A, Courvoisier S, Kasten J et al (2018) Fast high-resolution brain metabolite mapping on a clinical 3T MRI by accelerated 1H-FID-MRSI and low-rank constrained reconstruction. Magn Reson Med 81:2841–2857
27. Sartoretti T, Reischauer C, Sartoretti E, Binkert C, Najafi A, Sartoretti-Schefer S (2018) Common artefacts encountered on images acquired with combined compressed sensing and SENSE. Insights Imaging 9:1107–1115
28. Sharma SD, Fong CL, Tzung BS, Law M, Nayak KS (2013) Clinical image quality assessment of accelerated magnetic resonance neuroimaging using compressed sensing. Invest Radiol 48:638–645
29. Lee SH, Lee YH, Suh JS (2018) Accelerating knee MR imaging : compressed sensing in isotropic three- dimensional fast spin-echo sequence. Magn Reson Imaging 46:90–97
30. Altahawi FF, Blount KJ, Morley NP, Raithel E, Omar IM (2017) Comparing an accelerated 3D fast spin-echo sequence (CS-SPACE) for knee 3-T magnetic resonance imaging with traditional 3D fast spin-echo (SPACE) and routine 2D sequences. Skeletal Radiol 46:7–15